CrossMark

Subgrain Effect on Grain Scale Plasticity of NiTi Shape Memory Alloy Under Canning Compression: A Crystal Plasticity Finite Element Analysis

Li Hu[1] · Shuyong Jiang[2] · Jian Tu[1] · Zhiming Zhou[1]

Abstract

The subgrain effect of NiTi shape memory alloy during canning compression at 400 °C is investigated through electron back-scattered diffraction (EBSD) experiment, transmission electron microscope (TEM) experiment and crystal plasticity finite element (CPFE) simulation in explicit consideration of subgrain within each grain. Experimental investigations based on TEM and EBSD measurements confirm that the formation of subgrain actually results from the dislocation motion during canning compression. Numerical simulations based on the constructed polycrystalline models with various subgrains are used to investigate the subgrain effect during canning compression from a different point of view. In terms of texture evolution, subgrain effect does not change the tendency of texture evolution, but it contributes to the dispersed distribution with respect to the deformed grain/subgrain orientations. As for accumulative shear strain, subgrain effect contributes to sustaining larger plastic strain inside each grain, and it also results in the strain concentration near grain boundaries. With respect to von Mises stress, the subgrain effect facilitates the ease of stress concentration near grain boundaries and it contributes to possessing a homogeneous stress distribution within the inner part of each grain.

Keywords Shape memory alloy · Plastic deformation · Crystal plasticity · Finite element method

1 Introduction

Thanks to the crystallographically reversible phase transformations (i.e. B2 austenite phase to B19' martensite phase or B19' martensite phase to B2 austenite phase) occurring in NiTi shape memory alloy (SMA), NiTi SMA possesses outstanding shape memory effect and excellent superelasticity, and it has been widely used in the engineering field and materials science [1]. It is generally accepted that plastic deformation can serve as an efficient medium for making NiTi SMA ingots into wire, bar, tube strip and sheet [2–4]. In terms of manufacturing NiTi SMA products, hot plastic deformation plays a dominant role since NiTi SMA is difficult to form at room temperature because of its large strain hardening rate and high deformation resistance [5–7]. However, the microstructure of as-received NiTi SMA would be significantly affected and altered during plastic deformation by means of the competition between all active plastic deformation mechanisms, regardless of the adopted deformation condition. In general, these plastic deformation mechanisms are temperature-dependent and consist of stress-induced martensite phase transformation, dislocation slip/climb, deformation twinning, grain rotation and grain boundary slide/migration [8, 9]. Up to date, a broad agreement has been reached that the microstructure evolution during plastic deformation affects not only the shape memory effect and superelasticity of NiTi SMA, but also the mechanical properties of NiTi SMA [10, 11]. In particular, when NiTi SMA undergoes plastic deformation above the martensite desist temperature (M_d), it still possesses an unusual and high ductility (exceeding 30%) without the contribution of martensite

✉ Shuyong Jiang
  jiangshuyong@hrbeu.edu.cn

  Li Hu
  huli@cqut.edu.cn

  Jian Tu
  tujian@cqut.edu.cn

  Zhiming Zhou
  zhouzhiming@cqut.edu.cn

1 College of Material Science and Engineering, Chongqing University of Technology, Chongqing 400054, China

2 College of Mechanical and Electrical Engineering, Harbin Engineering University, Harbin 150001, China

transformation [12]. Microstructure evolution under this deformation condition undoubtedly occupies significant importance in terms of realizing such high ductility of NiTi SMA during plastic deformation. Hu et al. [13] has reported that when NiTi SMA undergoes plastic deformation at 400 °C (above M_d), plastic deformation contributes to the formation of subgrain which is encompassed by the low angle grain boundaries (LABs) with the misorientation of 5–15°. However, literature search indicates that investigations in terms of clarifying the nature and significance of the subgrain effect during plastic deformation of NiTi SMA are still scare. Consequently, it is of great importance to perform a specific investigation on the subgrain effect during plastic deformation of NiTi SMA for the purpose of illuminating its role during plastic deformation.

Because the dimension of subgrain falls into the grain scale, namely at least in the scale of micrometer, experimental approaches possess a certain limitation in illuminating the subgrain effect during plastic deformation. The aforementioned difficulty is expected to be resolved by means of crystal plasticity finite element method (CPFEM), which refers to the particular mechanical regime addressed by means of crystal plasticity (CP) theory as well as the approach on the basis of finite element method (FEM). At present, on the one hand, CPFEM has become a versatile simulation tool for clarifying plastic deformation mechanisms during plastic deformation, including dislocation slip, martensite transformation as well as deformation twinning [14]. On the other hand, CPFEM has the capability of providing high accuracy predictions on the intra-granular and inter-granular heterogeneities in polycrystal as well as texture evolution during plastic deformation [15, 16]. However, there seems to be no numerical study which specifically focuses on the subgrain effect during plastic deformation of NiTi SMA.

In the present study, the subgrain effect on the plastic deformation of NiTi SMA during canning compression at 400 °C is investigated by means of CPFEM. It has been generally accepted that the canned NiTi SMA sample is in the state of a three-dimensional stress by virtue of canning compression, contributing to sustaining large plastic deformation. The adopted cylinder polycrystalline models are constructed on the basis of electron back-scattered diffraction (EBSD) measurement of those deformed microstructures in the case of various deformation degrees. It is worth noting that the explicit construction of subgrain within all initial grains during numerical study has never been reported in the literature.

2 Materials and Methods

Firstly, the as-received NiTi SMA bar with its nominal composition of Ni50.9Ti49.1 (at%) is manufactured by means of vacuum induction melting method, followed by a hot rolling

at 800 °C. Subsequently, the NiTi SMA samples cut from the as-received NiTi SMA bar by virtue of electro-discharge machining (EDM) were canned into the low carbon steel cans. The detailed sample size is shown in Fig. 1. Afterwards, the NiTi SMA samples were compressed via the INSTRON-5500R universal testing machine equipped with a heating device at the deformation degree of 15%, 30%, and 45%, respectively, at the strain rate of 0.001 s^{-1} and at 400 °C. Finally, all deformed samples were quenched into water in order to keep their deformed microstructures.

Transmission electron microscope (TEM) experiment was conducted on the deformed NiTi SMA sample in the case of deformation degree of 45% in order to investigate the plastic deformation mechanism of NiTi SMA suffering from canning compression at 400 °C. Furthermore, EBSD experiments were applied to investigate the microstructure evolution of NiTi SMA samples at the deformation degree of 15%, 30%, and 45%, respectively. The detailed contents respect to the observation equipment used in TEM and EBSD measurement have been specified in the Ref. [13], as well as the specific procedure of TEM and EBSD sample preparation of NiTi SMA. Therefore, they would not be declared here. In addition, the selected observing region during TEM and EBSD measurement is in the central part of sample illustrated by a yellow box, as shown in Fig. 1.

3 Results and Discussion

3.1 Experimental Investigation on the Grain Scale Plasticity

Figure 2 shows the TEM observation of NiTi SMA sample suffering from canning compression at the deformation degree of 45% at 400 °C. It includes a TEM bright field image and the corresponding selected area electron
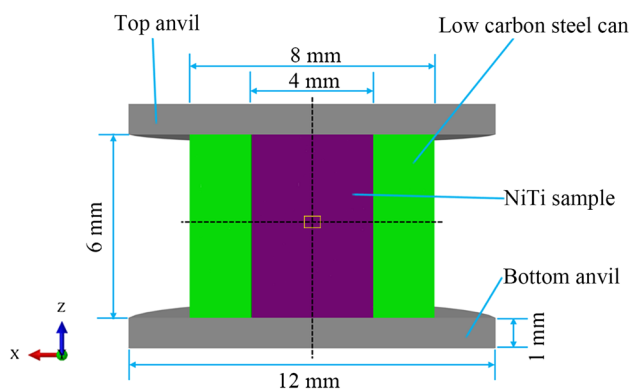

Fig. 1 Schematic diagram of NiTi SMA under canning compression, where the specified region compassed by the yellow box indicates the region used for TEM and EBSD measurements. (Color figure online)

diffraction (SAED) patterns in region B and region C. In Fig. 2a, the matrix of deformed NiTi SMA sample comprises many dense and tangled dislocations, and the distribution of dislocations within the deformed NiTi SMA sample is inhomogeneous. Figure 2b is the corresponding SAED pattern of region B and it demonstrates that the crystal structure of deformed NiTi SMA sample belongs to B2 austenite. In other words, phase transformation does not happen during canning compression at 400 °C. Moreover, in Fig. 2a, there exists a band region. Therefore, a SAED measurement is conducted in this band region and the corresponding result in Fig. 2c illustrates that the crystal structure in this band region also belongs to B2 austenite. This TEM observation indicates that deformation twinning dose not participate in the plastic deformation. Based on this experimental result and the reported deformation mechanisms of NiTi SMA above M_d [8], it is appropriate to conclude that dislocation slip serves as the main plastic deformation mechanism during canning compression of NiTi SMA at 400 °C.

Figure 3 demonstrates microstructure evolution and the corresponding maps of grain boundaries in the deformed NiTi SMA samples. It can be observed from Fig. 3a, c, e that with the progression of plastic deformation, there exists an increasing discrepancy in terms of orientation in different parts of individual grain. This phenomenon is attributed to the difference in terms of grain morphology and grain orientation contributing to the inhomogeneous plastic deformation at the grain scale during canning compression of NiTi SMA sample. As dislocation slip is the main carrier for sustaining plastic deformation during canning compression, the inhomogeneous plastic deformation within individual grain results in the heterogeneity in terms of dislocation initiation, multiplication and interaction. As a result, subgrains indicated by the red lines are gradually formed and heterogeneously distributed within the NiTi SMA sample and the number of subgrains increases with the increasing plastic deformation, as shown in Fig. 3b, d, f. It is worth noting that in the present study, the 5° criterion is applied in order to exclude the artificial substructure.

Fig. 2 TEM micrographs of NiTi SMA sample suffering from canning compression at the deformation degree of 45%: **a** bright field image; **b** SAED pattern in region B of **a**; **b** SAED pattern in region C of **a**
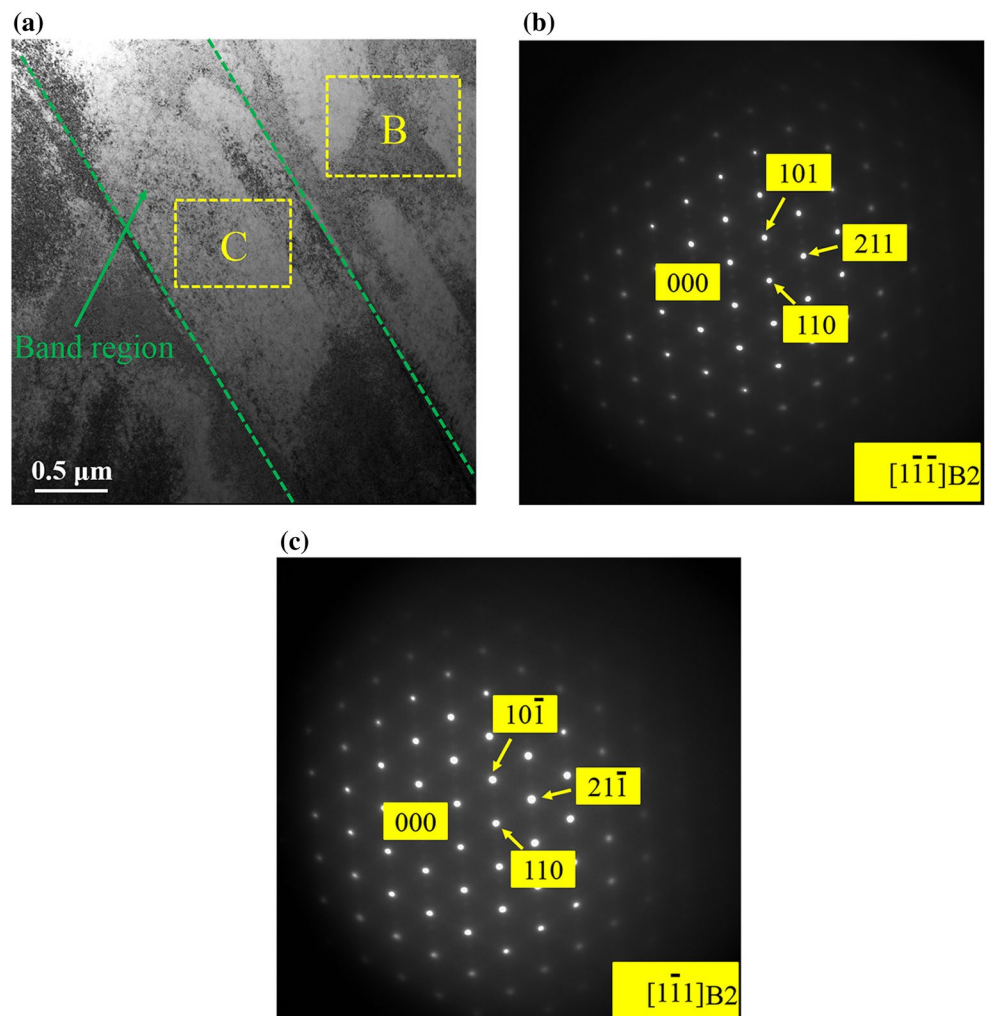
Fig. 3 Microstructure evolution and the corresponding evolution of grain boundaries at various deformation degrees: **a**, **b** 15%; **c**, **d** 30%; **e**, **f** 45%, respectively. The high angle grain boundaries (HABs) with the misorientation greater than 15° are represented by the blue lines, whereas the low angle grain boundaries (LABs) with the misorientation of 5–15° are illustrated by the red lines. (Color figure online)
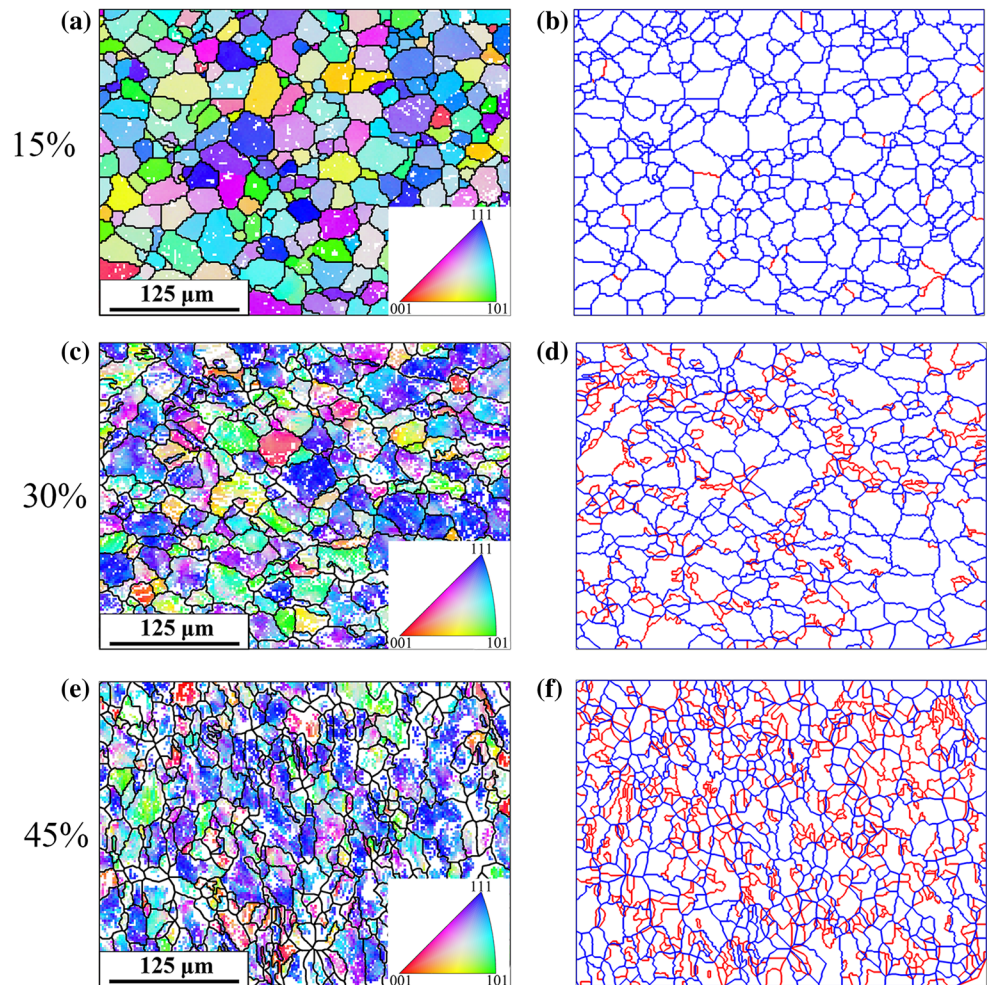

3.2 Numerical Investigation on the Grain Scale Plasticity

3.2.1 Establishment of Polycrystalline Model

The aim in the present study is to study the subgrain effect on the grain scale plasticity of polycrystalline NiTi SMA under canning compression. Therefore, it is necessary to explicitly construct the polycrystalline model which contains subgrains. Based on the aforementioned EBSD observation, the polycrystalline model is constructed by virtue of a free open source software package NEPER [17], as shown in Fig. 4. In NEPER, multiscale tessellations can be generated and therefore subgrains can be constructed within each grain. In the present study, four different polycrystalline models are constructed according to the number of subgrains within each grain. The first polycrystalline model is termed as 36-0-Model and it comprises 36 grains and does not have any subgrains within each grain. The second polycrystalline model is termed as 36-4-Model and it comprises 36 gra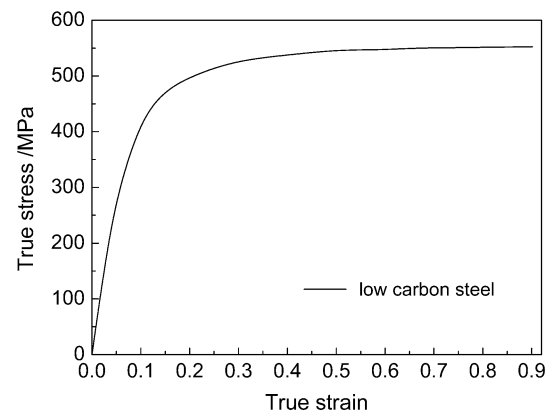ins and has 4 subgrains within each grain. The third polycrystalline model is termed as 36-8-Model and it comprises 36 grains and it possesses 8 subgrains within each grain. The fourth polycrystalline model is termed as 36-12-Model and it comprises 36 grains and consists of 12 subgrains within each grain. Moreover, those four polycrystalline models are meshed with the 4-node linear tetrahedron (C3D4) element. The mesh density within each grain/subgrain is about 2000 and this operation is realized by controlling the mesh size parameters in NEPER, contributing to eliminating the effect of mesh density on the numerical simulation. In the case of canning compression, theses constructed polycrystalline models are further canned in the low carbon steel cans whose inner diameter is the same with the diameter in the constructed models and the outer diameter is twice the diameter in the constructed models. The loading rate of canning compression is set to be 0.001 s^{-1} which is the same as the experimental loading rate. Moreover, the elastic and plastic data used for low carbon steel is obtained from the measured stress–strain curve in the case of uniaxial compression at the constant strain rate of 0.001 s^{-1} at 400 °C, as shown in Fig. 5.
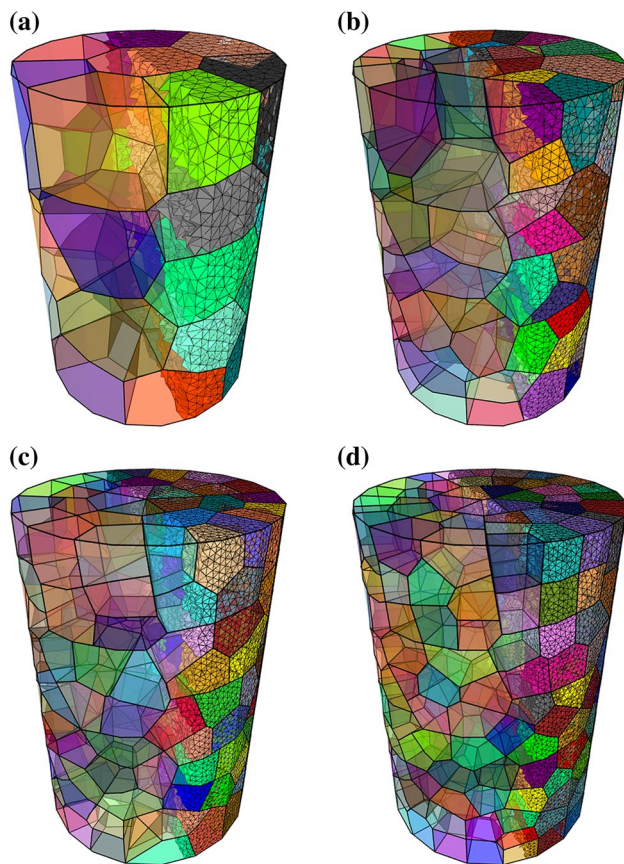
Fig. 4 Schematic diagrams of four polycrystalline models: **a** 36-0-Model; **b** 36-4-Model; **c** 36-8-Model; **d** 36-12-Model. (Color figure online)

Fig. 5 Stress-strain curve of low carbon steel subjected to uniaxial compression at 400 °C with a constant strain rate of 0.001 s^{-1}

3.2.2 Crystal Plasticity Model

Due to the aforementioned TEM and EBSD investigations, dislocation slip is the main plastic deformation mechanism during canning compression at 400 °C. Phase transformation and deformation twinning do not participate in plastic deformation. Therefore, the modeling framework used to determine the polycrystalline plastic deformation in the present study depends on only dislocation slip. Various slip modes including {110}<111>, {110}<100> and {010}<100> are incorporated into the crystal plasticity finite element model in order to accommodate arbitrary plastic deformation [8, 18, 19]. The framework of the current crystal plasticity model was initially developed by Huang [20] to capture slip-based plastic deformation. The corresponding crystal plasticity theory and numerical implementation are well documented in the Ref. [19], as well as the employed material parameters for NiTi SMA at 400 °C. Therefore, the corresponding contents are not repeated in the present study in order to reduce the length of the paper. It is worth mentioning that in the present study, the same set of material parameters is used in all four constructed polycrystalline models, although

the actual situation is not the case. For instance, compared to the 36-0-Model, the 36-12-Model obviously happens in the case of a larger deformation degree. Therefore, a set of material parameters with larger value should be used in the case of the 36-12-Model. The application of the same set of material parameters in the present study contributes to making a direct comparison between all four constructed polycrystalline models.

3.2.3 Texture Evolution During Canning Compression

It has been generally accepted that initial texture has an important influence on the activities of deformation mechanisms inside individual grain during plastic deformation. Therefore, prior to performing the numerical simulations on the basis of these four constructed polycrystalline models, the orientation of each grain/subgrain needs to be confirmed. In the present study, an accurate orientation characterization method based on Euler angle (ϕ_1, φ, ϕ_2) is applied to characterize the grain/subgrain orientation within each polycrystalline model. The grain/subgrain orientations corresponding to the 36-0-Model polycrystalline model is shown in Fig. 6a and they are randomly generated. Subgrain inside each grain is with LAGs between neighboring grains/subgrains. In the present study, a methodology provided by Han et al. [21] is applied and a random rotation angle in the range of 5–15° is generated. Then, the rotation is conducted via changing the third Euler angle ϕ_2. Through this kind of rotation, grain/subgrain orientations in the case of the 36-4-Model polycrystalline model, the 36-8-Model polycrystalline model and the 36-12-Model polycrystalline model are finally formed. Figure 6b illustrates the grain/subgrain orientations in the case of the 36-12-Model polycrystalline model and it is obvious that there exists a slight difference between the poles of grains and the poles of subgrains.

Fig. 6 Pole figures of initial microstructure in **a** the 36-0-Model polycrystalline model and **b** the 36-12-Model polycrystalline model. (Color figure online)
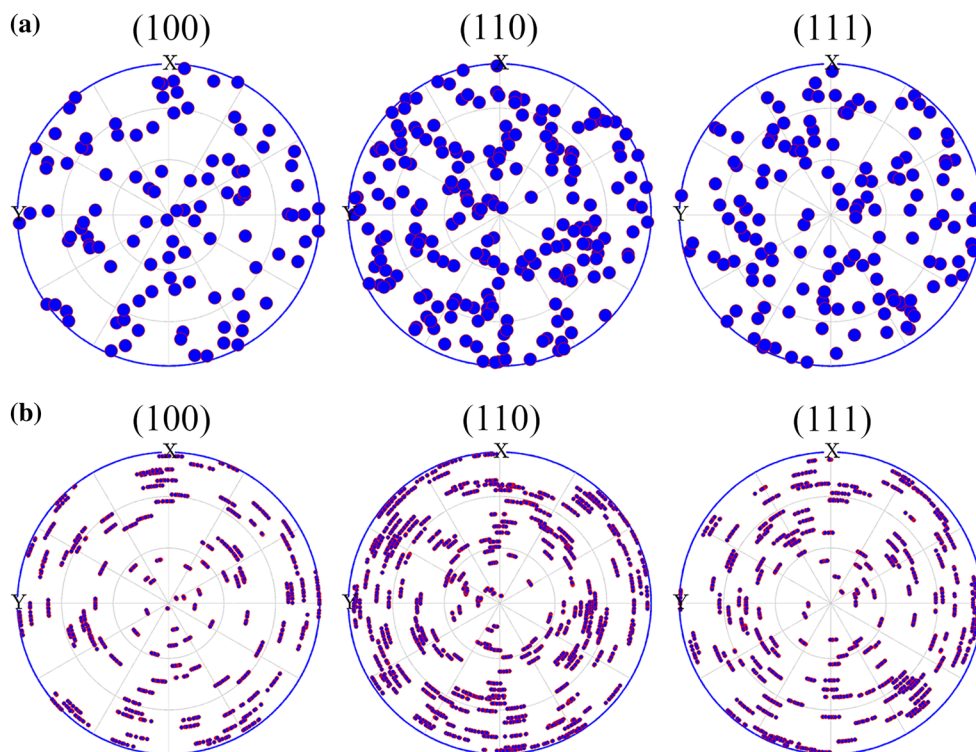
To compare the predicted texture evolution resulting from canning compression, crystal orientations of these four polycrystalline models at the applied deformation degree of 10% are plotted within the unit stereographic triangle. Every datum point in the stereographic triangle corresponds to grain/subgrain orientations obtained from the integration point of C3D4 element in the polycrystalline model. Figure 7 shows the predicted texture evolution of these four constructed polycrystalline models and it can be seen form Fig. 7 that the predicted deformed textures show reasonable agreement during canning compression. However, the spread in the initial grain/subgrain orientations in the four constructed polycrystalline models results in an increasing tendency of dispersed distribution with respect to the deformed grain/subgrain orientations.
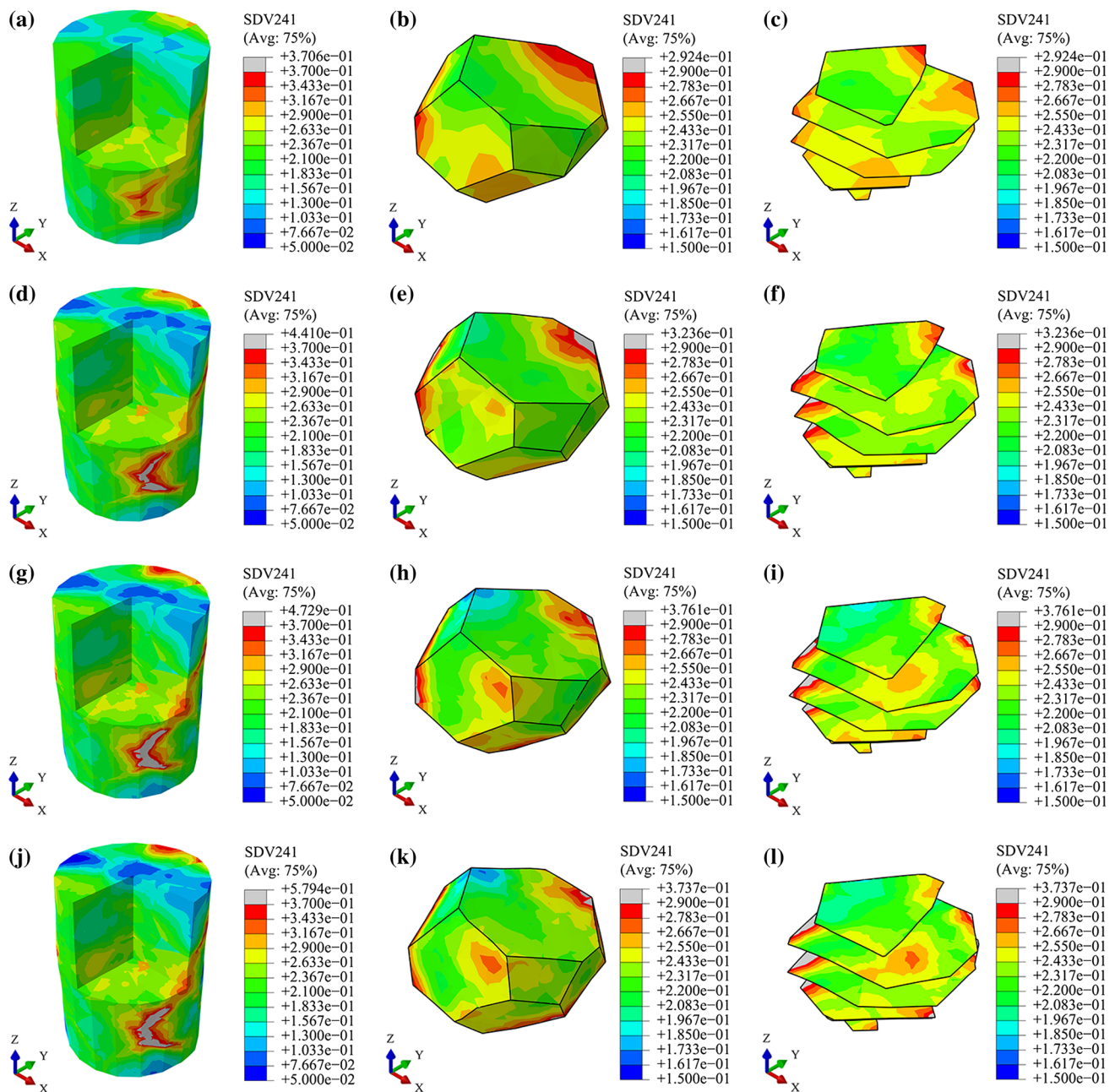
3.2.4 Distribution of Accumulative Shear Strain

Figure 8 illustrates the distribution of accumulative shear strain in the constructed polycrystalline model as well as the No. 36 grain inside the constructed polycrystalline model at the deformation degree of 10%. The accumulative shear strain is sum of shear strain with respect to all activated slip systems during plastic deformation and is termed as SDV 241 in the numerical simulation. As shown in Fig. 8, the accumulative shear strain is heterogeneously distributed within these four constructed polycrystalline models during canning compression. With the increase in the number of subgrains within each grain, some regions inside
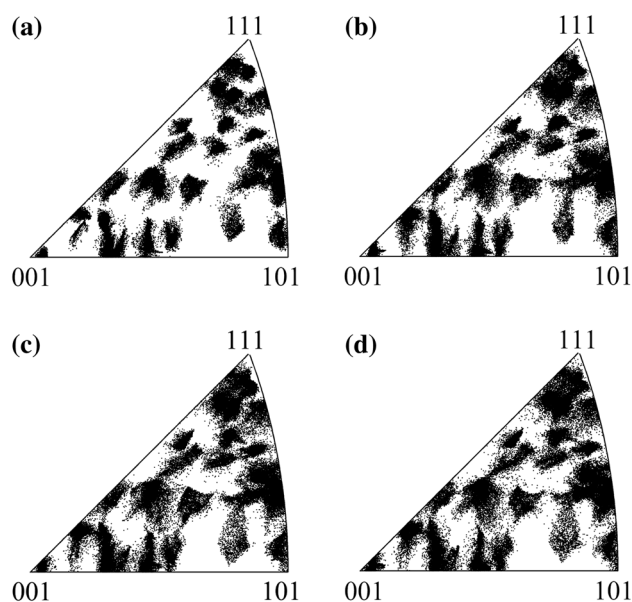
Fig. 7 CPFEM predictions of the deformed grain/subgrain orientations at the deformation degree of 10%: **a** in the 36-0-Model polycrystalline model; **b** in the 36-4-Model polycrystalline model; **c** in the 36-8-Model polycrystalline model; **d** in the 36-12-Model polycrystalline model

the polycrystalline model sustain less plastic deformation, whereas some regions suffer from more plastic deformation. In No. 36 grain inside the polycrystalline mode, along with the increasing subgrains inside each grain, the inner part of

Fig. 8 Distribution of accumulative shear strain in the constructed polycrystalline model and in No. 36 grain inside the constructed polycrystalline model at the defo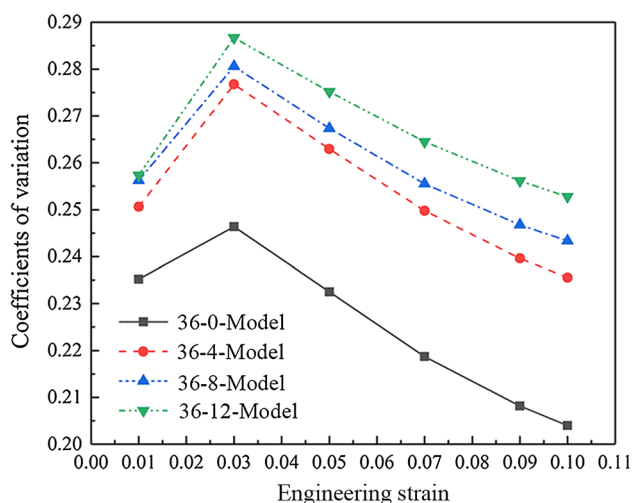rmation degree of 10%: **a–c** in the 36-0- Model polycrystalline model; **d–f** in the 36-4-Model polycrystalline model; **g–i** in the 36-8-Model polycrystalline model; **j–l** in the 36-12-Model polycrystalline model. (Color figure online)

No. 36 grain and the outer part of No. 36 grain near the grain boundary are both with higher accumulative shear strain. This phenomenon demonstrates that the subgrain effect contributes to enhancing the plastic strain inside each grain during plastic deformation, and it can also result in the strain concentration near grain boundaries. Moreover, the distribution of accumulative shear strain in No. 36 grain is continuous and this observation illustrates that the strain field can go across the subgrain boundaries with LABs. Sachtleber

et al. [22] and Li et al. [23] have reported this similar result, indicating that the effect of LABs is less pronounced by comparison with the effect of HABs.

The statistical analysis of accumulative shear strain in the four constructed polycrystalline models at the deformation degree of 10% is also conducted and is shown in Fig. 9. In the present study, the coefficient of variation, which is defined as the ratio of standard deviation to mean value, is used in statistical analysis of data. As compared with

the standard deviation, the coefficient of variation can not only precisely grasp the discreteness of data, but also eliminate the influence of measurement scale and measurement dimension on statistical analysis. Large value of coefficient of variation corresponds to large no-uniformity of variable distribution, and vice versa. As shown in Fig. 9, the relationship between the coefficient of variation about accumulative shear strain and the engineering strain is similar in the four constructed polycrystalline models, namely the coefficient of variation about accumulative shear strain monotonically increases with the engineering strain, and a maximum value of coefficient of variation occurs at about 0.03 engineering strain. After that the coefficient of variation about accumulative shear strain decreases continuously with further plastic deformation. This observation result is correlated with the heterogenous plastic deformation at the grain scale. At the early stage of canning compression, individual grains within the constructed polycrystalline model deform heterogeneously, indicating that there exists significant difference with respect to the activation of various slip systems. When the constructed polycrystalline model sustains larger plastic deformation, multiple dislocation slip intensively occurs within individual grain and this contributes to reducing the coefficient of variation about accumulative shear strain. Moreover, it can be seen from Fig. 9 that with the increasing number of subgrains inside each grain, the polycrystalline model with more subgrains is with larger coefficient of variation about accumulative shear strain. This tendency can be explained using the observation in Fig. 8, where it can be noted that the subgrain effect contributes to sustaining

larger plastic strain inside each grain and it results in strain concentration near grain boundaries.

3.2.5 Distribution of von Mises Stress

Figure 10 illustrates the distribution of von Mises stress in the constructed polycrystalline model as well as the No. 36 grain inside the constructed polycrystalline model at the deformation degree of 10%. Reason for choosing the scale quantity of von Mises stress in the present study is that it can effectively and directly reflect the intensity of a three-dimensional stress state, and therefore it can provide valuable information from the complex three-dimensional stress state at any material point. As shown in Fig. 10, the von Mises stress is obviously heterogeneously distributed in these constructed polycrystalline models. Moreover, in No. 36 grain the stress concentration near grain boundary is gradually relieved with the increment in the number of subgrains, whereas the inner region inside No. 36 grain tends to possess a homogeneous stress distribution with the increasing number of subgrains. Consequently, this observation confirms that the subgrain effect during plastic deformation facilitates the ease of stress concentration near grain boundaries as well as the inhomogeneity within the inner part of each grain. The aforementioned observation is further enhanced by the statistical analysis of von Mises stress, as shown in Fig. 11. It is obvious that the evolution of the coefficient of variation about von Mises stress is quite similar to the evolution of the coefficient of variation about accumulative shear strain. This observation can also be due to the heterogeneous plastic deformation at the grain scale. At the early stage of canning compression, individual grains with harder and softer orientations reach correspondingly higher and lower level of stress, respectively. This contributes to the increase of the coefficient of variation about von Mises stress. However, with the further progression of plastic deformation, the as-received various grain orientations gradually rotate and concentrate to some specific orientations, forming a texture during plastic deformation. As a result, the difference in mechanical response of individual grain gradually decreases, so does the coefficient of variation about von Mises stress as well. Moreover, it can be seen from Fig. 11 that the coefficient of variation about von Mises stress possesses a tendency of increase on the basis of the increasing subgrains within the constructed polycrystalline models. The aforementioned phenomenon is undoubtedly attributed to the subgrain effect during plastic deformation. On the one hand, subgrain effect contributes to the compatible deformation inside each grain, so stress concentration within each grain is avoided and the inner part of each grain possesses a homogeneous stress distribution. On the other hand, the fluctuation in terms of subgrain orientation benefits the compatible deformation with neighboring grain/subgrain and thus contributes to the mitigation of stress concentration near grain boundaries. Another interesting
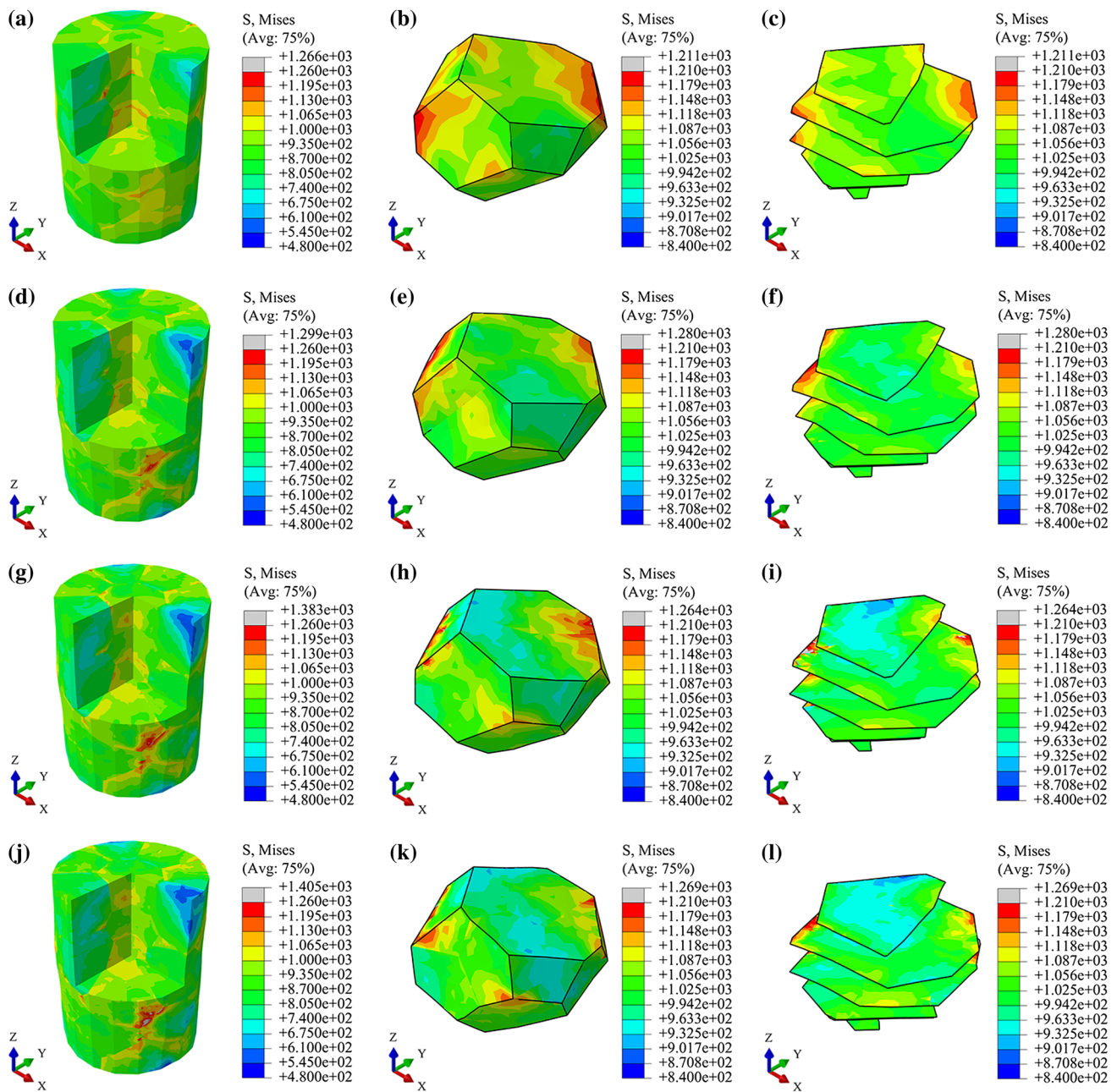
Fig. 9 Statistical analysis of accumulative shear strain in the constructed polycrystalline models suffering from canning compression at the deformation degree of 10%: relationship between the coefficient of variation about accumulative shear strain and the engineering strain. (Color figure online)
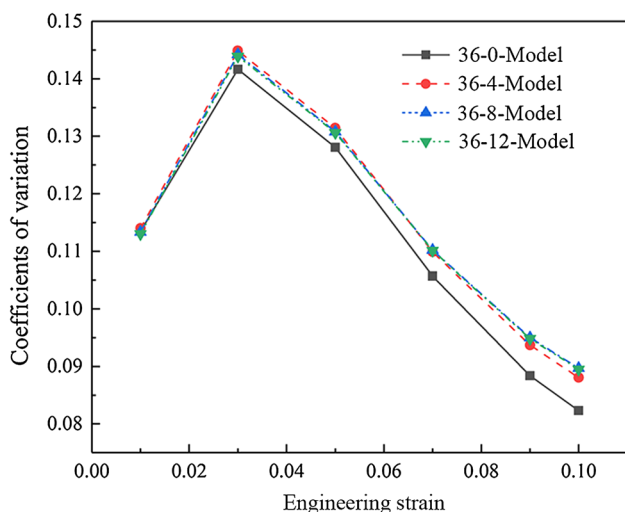
Fig. 10 Distribution of von Mises stress in the constructed polycrystalline model and in No. 36 grain inside the constructed polycrystalline model at the deformation degree of 10%: **a**–**c** in the 36-0-Model polycrystalline model; **d**–**f** in the 36-4-Model polycrystalline model; **g**–**i** in the 36-8-Model polycrystalline model; **j**–**l** in the 36-12-Model polycrystalline model. (Color figure online)

observation result is that the coefficient of variation about von Mises stress shows little sensitivity to the number of subgrains. This phenomenon is mainly attributed to the fact that in the present study, the same set of material parameters is used and this diverges from the actual situation. Therefore, there are small differences in mechanical response of individual grain within all four constructed polycrystalline models, which results in the minor sensitivity of the coefficient of variation about von Mises stress to the number of subgrains.

4 Conclusions

Experimental investigations based on TEM and EBSD measurements confirm the formation of subgrain, which results from the dislocation motion during canning compression. Then the crystal plasticity finite element simulations based on the constructed polycrystalline models in explicit consideration of subgrains within each grain are conducted in order to investigate the subgrain effect on plastic deformation of

Fig. 11 Statistical analysis of von Mises stress in the constructed polycrystalline models suffering from canning compression at the deformation degree of 10%: relationship between the coefficient of variation about von Mises stress and the engineering strain. (Color figure online)

NiTi SMA during canning compression at 400 °C, the following conclusions can be drawn.

1. The subgrain effect does not change the tendency of texture evolution during canning compression. However, the spread in the initial grain/subgrain orientations results in the dispersed distribution with respect to the deformed grain/subgrain orientations.
2. The subgrain effect contributes to sustaining larger plastic strain inside each grain during canning compression, and it also results in the strain concentration near grain boundaries.
3. The subgrain effect facilitates the ease of stress concentration near grain boundaries during canning compression and it contributes to possessing a homogeneous stress distribution within the inner part of each grain.

References

1. L. Wang, C. Wang, L.C. Zhang, L. Chen, W. Lu, D. Zhang, Sci. Rep. **6**, 23905 (2016)
2. A. Isalgue, C. Auguet, R. Grau, V. Torra, N. Cinca, J. Fernandez, J. Mater. Eng. Perform. **24**, 3323–3327 (2015)
3. Y. Liu, Acta Mater. **95**, 411–427 (2015)
4. E. Twohig, P. Tiernan, J. Butler, C. Dickinson, S. Tofail, Acta Mater. **68**, 140–149 (2014)
5. K. Gall, J. Tyber, G. Wilkesanders, S.W. Robertson, R.O. Ritchie, H.J. Maier, Mater. Sci. Eng. A **486**, 389–403 (2008)
6. S. Manchiraju, D. Gaydosh, O. Benafan, R. Noebe, R. Vaidyanathan, P.M. Anderson, Acta Mater. **59**, 5238–5249 (2011)
7. K. Kazemi-Choobi, J. Khalil-Allafi, V. Abbasi-Chianeh, Mater. Sci. Eng. A **551**, 122–127 (2012)
8. O. Benafan, R. Noebe, S. Padula, A. Garg, B. Clausen, S. Vogel, R. Vaidyanathan, Int. J. Plast. **51**, 103–121 (2013)
9. L. Hu, S. Jiang, Y. Zhang, Y. Zhao, S. Liu, C. Zhao, Intermetallics **70**, 45–52 (2016)
10. H.M. Paranjape, S. Manchiraju, P.M. Anderson, Int. J. Plast. **80**, 1–18 (2016)
11. F. Weafer, Y. Guo, M. Bruzzi, J. Mech. Behav. Biomed. **53**, 210–217 (2016)
12. T. Duerig, Mater. Sci. Eng. A **438**, 69–74 (2006)
13. L. Hu, S. Jiang, Y. Zhang, Metals **7**, 356 (2017)
14. F. Roters, P. Eisenlohr, L. Hantcherli, D.D. Tjahjanto, T.R. Bieler, D. Raabe, Acta Mater. **58**, 1152–1211 (2010)
15. H. Sheikh, R. Ebrahimi, E. Bagherpour, Mater. Des. **109**, 289–299 (2016)
16. H. Sheikh, R. Ebrahimi, J. Mater. Sci. **51**, 10178–10190 (2016)
17. R. Quey, P. Dawson, F. Barbe, Comput. Method. Appl. M **200**, 1729–1745 (2011)
18. L. Hu, S. Jiang, T. Zhou, J. Tu, L. Shi, Q. Chen, M. Yang, Materials **10**, 1172 (2017)
19. L. Hu, S. Jiang, Y. Zhang, D. Sun, Met. Mater. Int. **23**, 1075–1086 (2017)
20. Y. Huang, *A user-material subroutine incorporating single crystal plasticity in the ABAQUS finite element program* (Harvard University, Cambridge, 1991)
21. F. Han, B. Tang, H. Kou, J. Li, Y. Feng, Prog. Nat. Sci. Mater. Int. **25**, 58–65 (2015)
22. M. Sachtleber, Z. Zhao, D. Raabe, Mater. Sci. Eng. A **336**, 81–87 (2002)
23. L.T. Li, Y. Lin, L. Li, L.M. Shen, D.X. Wen, J. Mater. Eng. Perform. **24**, 1294–1304 (2015)